Supporting Information for:

Spin-dependent exciton quenching and spin coherence in CdSe/CdS nanocrystals

K. J. van Schooten[1], J. Huang[2], W. J. Baker[1], D. V. Talapin[2, 3], C. Boehme[1 *] and J. M. Lupton[1, 4 *]

[1] Department of Physics and Astronomy, University of Utah, 115 South 1400 East, Salt Lake City, Utah 84112, USA

[2] Department of Chemistry, University of Chicago, Chicago, Illinois 60637, USA

[3] Center for Nanoscale Materials, Argonne National Laboratory, Argonne, Illinois 60439, USA

[4] Institut für Experimentelle und Angewandte Physik, Universität Regensburg, D-93040 Regensburg, Germany

Experimental Methods

The tetrapod nanocrystals consist of wurtzite CdS arms approximately 20 nm in length and 6 nm in diameter, grown onto four faces of zincblende CdSe cores of 4 nm diameter. Synthesis details are given in Ref. 1. The same batch of CdSe cores which was used to seed tetrapod growth was also investigated alone for comparison, as shown in Figure 2b) of the main text. Each series of colloidal nanoparticles used in these measurements was first diluted into a toluene Zeonex (Zeon Chemicals L.P.) solution and then drop cast into a small Teflon bucket (2mm × 3mm). Upon solvent evaporation, a solid matrix was formed, which is both optically and paramagnetically inert, but contains the distributed nanoparticles. The sample was then suspended in a He flow cryostat containing a dielectric microwave resonator, generally kept at 3.5K for all measurements, except for Rabi nutation experiments which was performed at 15K. Optical access to the sample was made by extending a home-built fiber bundle through a cryostat port and into the resonator, resting at the mouth of the Teflon sample bucket. A c.w. Ar^+ laser, tuned to 457.9 nm (2.708

* Corresponding authors. Email: john.lupton@physik.uni-regensburg.de ; boehme@physics.utah.edu

eV) and combined with a suitable filter to remove spontaneous emission (Semrock Maxline), was passed into a single fiber and used to excite the nanocrystal ensemble with 20mW of power (intensity approximately 85 $\mu W \cdot cm^{-2}$). The remainder of the fibers were used to collect PL, from which scattered laser light was filtered out with a 458 nm ultrasteep long-pass filter (Semrock RazorEdge). Specific emission bands for each nanoparticle ensemble were spectrally selected by choosing an appropriate filter set: the CdS nanorod and CdSe core deep-level defect emission were isolated with a 550 nm (2.254 eV) long-pass filter (ThorLabs); the CdS nanorod band-edge emission was cut with a 460±2 nm (2.695±0.012 eV) narrow-band filter (ThorLabs); the tetrapod core emission was picked with a 620±2 nm (2.000±0.007 eV) narrow-band filter (ThorLabs).

The selected PL was focused onto a low-noise photodiode (Femto LCA-S-400-Si), whose signal was amplified with a Stanford Research Systems low-noise preamplifier (SR560). AC coupling of the input signal was used in order to apply gain to only the modulated contribution of the PL intensity. A 300Hz high-pass frequency filter was also applied in order to help isolate the transient response of the ODMR signal from spurious electrical and optical modulations.

With sufficient gain applied, the resulting signal was passed into the fast digitizer of a Bruker SpecJet contained within an Elexsys E580 system, which correlates the timing of the microwave pulse sequence with the transient response. Programmable control over pulse routine timing, leveling of the external magnetic field and signal acquisition was utilized to carry out the large number of measurements required for each data set. For example, the transient mappings displayed in Fig. 2c),d),f), and h) required an X-band (9.8 GHz) microwave pulse of 800ns duration to be applied every 800 μs a total of 16384 times. The transient responses of the individual measurements were added together before incrementing the external magnetic field B_0. For the high-resolution time transients shown in Fig. 3b),d), the microwave shot repetition rate was set to be greater than 2ms, much longer than the full relaxation time to steady-state populations of carrier states under constant excitation of the material system. Rabi oscillations were obtained by monitoring the amplitude of the transient PL response as a function of microwave pulse

length. The transit times for driving the system from optically dark to optically bright states served as useful timing information needed for constructing the π and $\pi/2$ pulses of the Hahn echo sequence. A full description of this conventional pulse sequence, as used in ODMR, is given below.

Band-edge trap states in CdS nanocrystals

The existence of trap states lying very close to the band gap of our primary material system of interest, the CdS nanorods, can easily be confirmed by considering the luminescence decay characteristics following an optical excitation pulse. A sample similar to that used for the ODMR experiments is fabricated, consisting of nanorods suspended in a polystyrene block several microns thick. This sample is mounted, under vacuum, to the cold-finger of a closed-cycle Helium cryostat, which cools to 21 K. A diode laser operating at 355 nm (3.493 eV) with nanosecond pulse length and variable repetition rate is used as an excitation source. PL spectra are monitored with a gated, intensified CCD (ICCD) camera mounted to a spectrometer, allowing us to record the decay of emission intensity as a function of gating time following optical excitation. The prompt PL is shown in Figure S1. The dashed green line in panel a) indicates the spectral position which is monitored as a function of time. As is seen in panel b), the PL intensity drops off approximately following a power law over five orders of magnitude in time. The excitonic emission spectrum does not shift significantly over this time.

The accepted physical mechanism responsible for delaying emission in these nanoparticles for such long times is the temporary isolation of the optically excited charge carriers into their respective "trap" states[1], dramatically decreasing the amount of wavefunction overlap of the electron-hole pair, and therefore the likelihood of recombination. As the detrapping rate back into the band-edge excitonic states depends exponentially on the trap energy, which in turn is distributed exponentially, a distribution of detrapping rates is observed across the nanoparticle ensemble, leading to the power law-like emission decay[2].

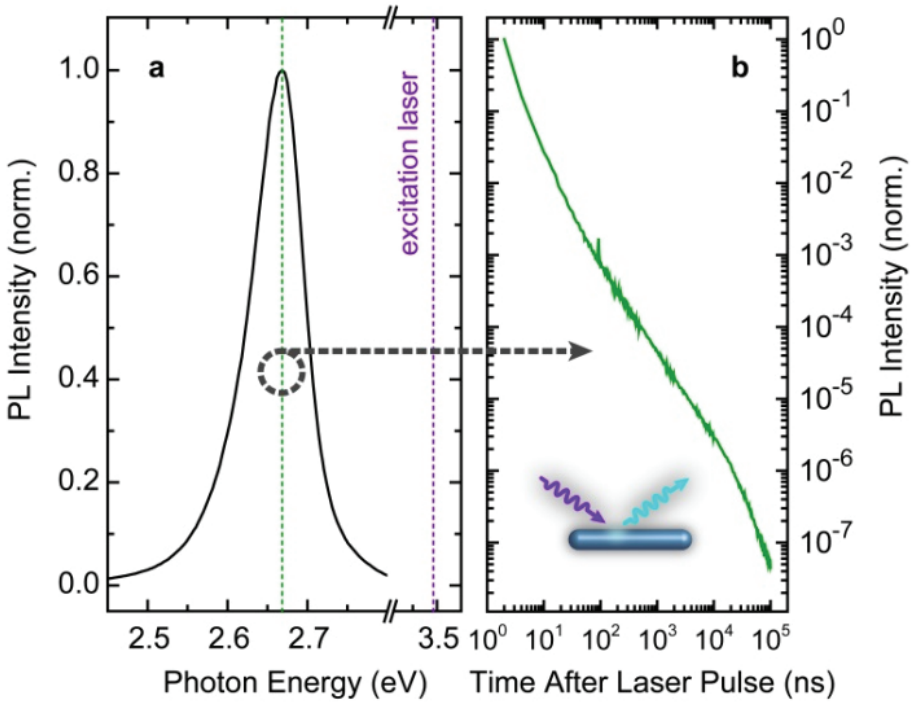

Figure S1: a) Prompt band-edge PL spectrum of CdS nanorods at 21 K following excitation with a 355 nm (3.493 eV) laser pulse. b) The emission peak is monitored as a function of delay time from excitation using a gated ICCD camera and spectrometer. The peak emission decay approximately follows a power law, revealing the presence of long-lived "trap" states, which are energetically close to the semiconductor band edge where the exciton forms.

Correlation of resonances

To determine which of the three resonances seen in the tetrapods and nanorods (Fig. 3) correspond to a coupled pair of carriers, the time dynamics of the resonances are considered. The correlation of the features in time dynamics in Fig. 3 is independent of temperature and laser power, although both of these parameters directly affect the transient response. The biexponential time dynamics shown in Fig. 3b,d) are characteristic of a (electron-hole) pair process, which has been investigated extensively in the context of conjugated polymers[3].

While the observation of identical dynamics (Fig. 3) alone is sufficient to conclude that each of these paramagnetic centers belong to the same coupled system[3], further proof derives from a comparison of the

areas of the two features. Since the area of each resonance represents the probability of inducing a spin transition which causes an optical activity, separately resonant carriers belonging to the same excitation (e.g. an electron and a hole in a pair) must exhibit equal probabilities for this process to occur. To aid in the analysis of comparing the equality of these probabilities, a fitting routine employing three Gaussians was utilized to study the transient spectra. For the CdS nanorod band-edge emission, the results of this analysis are shown in Figure S2. A correlation of the $g \sim 2.00$ and $g \sim 1.84$ resonances is clear since the fitting routine finds comparable areas for the Gaussians representing these two features over a wide range of times. Additionally, we note that the central $g \sim 1.95$ resonance must represent a carrier state which is completely decoupled from the neighboring resonances since it displays marked differences in both probability (i.e. area of the resonance) and time dynamics.

A further point must be made about the disparity between the T_2 times given for each of these carriers in Fig. 4) in the main text. The results of the Hahn echo experiment (outlined below) on the $g \sim 1.84$ center of the CdS nanorods give a phase coherence time which is nearly half that of the $g \sim 2.00$ center, as would be expected for a carrier experiencing a larger degree of spin-orbit coupling. The inequality between T_2 times of the two (correlated) carriers reflects the unique chemical environments of each and does not conflict with the assignment of the two centers as representing a coupled pair. In fact, and although not measured explicitly, the only hard requirement imposed on the spin states of the pair is that each are characterized by identical T_1 times, which is inferred from the equal time dynamics of each resonance[3].

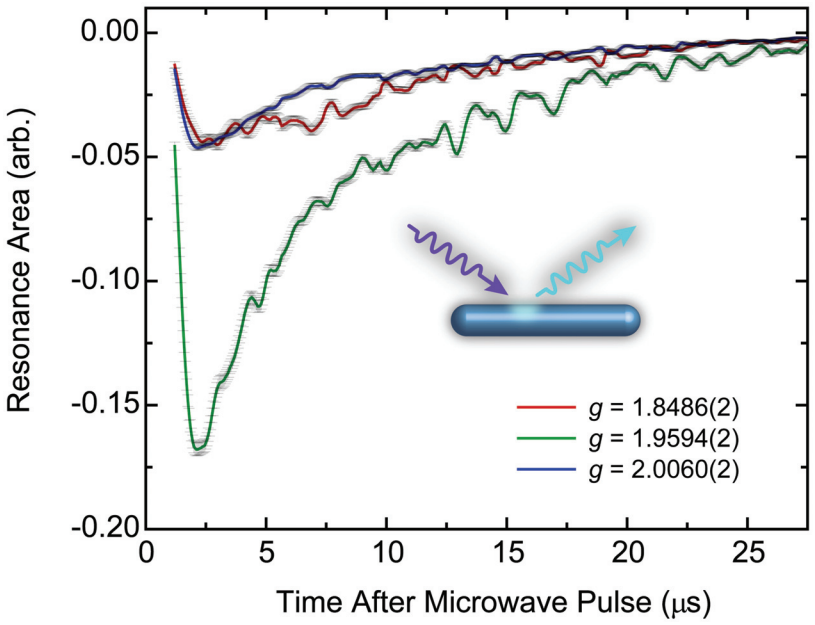

Figure S2: Integrated resonances (areas) as a function of time obtained from the triple Gaussian fit applied to the ODMR mapping of CdS nanorod band-edge emission. The equal resonance areas for the $g \sim 2.00$ and $g \sim 1.84$ sites denote the equal probabilities of inducing optical activity following a microwave-induced spin transition. Since the probabilities of inducing such a transition for each of the two sites are equal, it can be concluded that they represent a coupled pair of trap states (i.e. weakly-bound electron-hole pair). The $g \sim 1.95$ state is clearly unrelated.

Spin identity of trap states and mutual interactions in carrier pairs

Determining spin identity is a crucial step in chemical fingerprinting as it can help to ultimately illuminate the chemical nature of a trap state for a specific carrier. For example, the complementary knowledge of spin multiplicity, resonance *g*-factor and resonance structure can help to establish the exact symmetry of a paramagnetic site and therefore the exact environment of the localized carrier.

The spin identity of a paramagnetic center can be confirmed in a straightforward manner by carrying out a Rabi nutation experiment since the carrier's spin quantum number is directly reflected in the frequency of oscillation between mutual spin configurations. For transitions between Zeeman-split m_s levels of the

form $|S, m_s - 1\rangle \rightarrow |S, m_s\rangle$, and neglecting any significant detuning from resonance, the Rabi frequency is determined by[4] $\Omega_R = \sqrt{S(S+1) - m_s(m_s - 1)} \cdot \gamma B_1$, where $\gamma = \frac{g\mu_B}{\hbar}$ is the gyromagnetic ratio for the center, μ_B is the Bohr magneton, $\hbar$ is Planck's constant, and B_1 is the microwave-induced magnetic field strength at the sample position within the microwave resonator. The *g*-factor is experimentally determined by the resonance center, but once the Rabi nutation has been recorded, a precise value for B_1 must be obtained in order to confirm the spin multiplicity of the trap site.

An additional material serving as a standard paramagnetic center with known *g*-factor and spin can be loaded into the microwave resonator alongside the material of interest; in this case, phosphorus-doped crystalline silicon (Si:P with a doping concentration of $[^{31}P] = 10^{16} cm^{-3}$). The variations in microwave-induced magnetic field within the resonator volume that contains the combined sample are negligible over the few millimeters of sample breadth, allowing for the direct determination of B_1 fields experienced at the trap sites of the nanorods through recording of the Rabi frequency of ^{31}P centers in Si.

Aside from establishing the spin identity of the $g \sim 2.00$ and $g \sim 1.84$ sites, we are also interested in the type of mutual interactions experienced by the two carriers. Again, by scrutinizing the frequency components of the Rabi oscillations, general statements can be made as to the prevailing nature of intra-pair coupling. The on-resonance spin-½ system precesses at a frequency of $\Omega_R = \gamma B_1$. As additional, non-negligible interaction terms are introduced into the Hamiltonian describing the spin pair, further frequency components mix with Ω_R which directly correspond to specific forms of interactions. It has previously been shown[5] that increasing exchange interactions leads to frequency components of $2\gamma B_1$ appearing in the Rabi flopping signal, while an increase in dipolar interactions results in components of[6] $\sqrt{2}\gamma B_1$.

On the other hand, the same frequency components may arise not due to any particular pair interaction, but merely from spin transitions being stimulated within a particular spin manifold. For example, a $\left|\frac{3}{2},-\frac{1}{2}\right\rangle \rightarrow \left|\frac{3}{2},\frac{1}{2}\right\rangle$ transition will produce a Rabi frequency component of $2\gamma B_1$, while a strongly exchange-coupled spin-½ system can do the same. This approach of attributing a systematic cause to a measured frequency component is made ambiguous if both the spin identity and the interaction type remain unresolved for the paramagnetic center. There is, however, one case where this ambiguity is easily resolved, which is for the spin-½ pair experiencing weak exchange and dipolar interactions. In this case, the only frequency component present in the Rabi nutation is γB_1, which is the case at hand.

Shown in Fig. S3 are Fourier transforms of the Rabi oscillations in Fig. 4a) ($g \sim 1.84$) and Fig. 4b) ($g \sim 2.00$) of the main text. We focus solely on data obtained from the CdS nanorods to investigate the spin state and any possible interactions within the pair since the observed ODMR intensities of the nanorods are an order of magnitude larger than the same transitions seen in the tetrapods. The absence of any additional frequency components in the Fourier spectrum besides the γB_1 fundamental implies that this spin-dependent transition results from a pair of weakly-coupled spin-½ carriers, where both exchange and dipolar couplings are negligible. This weak coupling is not beyond expectations for such localized carriers since the distribution of trap sites over the nanoparticles should be random in space, leaving an average pair separation too large for either sufficient wavefunction overlap (exchange) or magnetic dipole-dipole interactions. Such weakly-bound precursor states, which ultimately feed into tightly-bound band-edge excitonic states, are common amongst a variety of material systems, such as hydrogenated amorphous silicon[6] and organic semiconductors[7] and can be manipulated through ESR in order to predetermine the permutation symmetry of final tightly-bound states.

In this case, the carriers comprising this weakly-bound precursor state are each spin-½, which means that they form mutual spin states that can be characterized as either singlet or triplet. This holds for the trapped carriers only, as the band-edge excitonic states are well known to have a higher spin-multiplicity[8].

Therefore, upon detrapping, the singlet/triplet nature of the trapped pair will be projected upon the five individual spin states which make up the exciton fine structure. Since three of these states are bright and two are dark (i.e. spin allowed and forbidden optical transitions), changing the singlet/triplet nature of the trapped carriers will change the probability of moving back into a bright or dark state after detrapping occurs, thereby changing the overall exciton state populations.

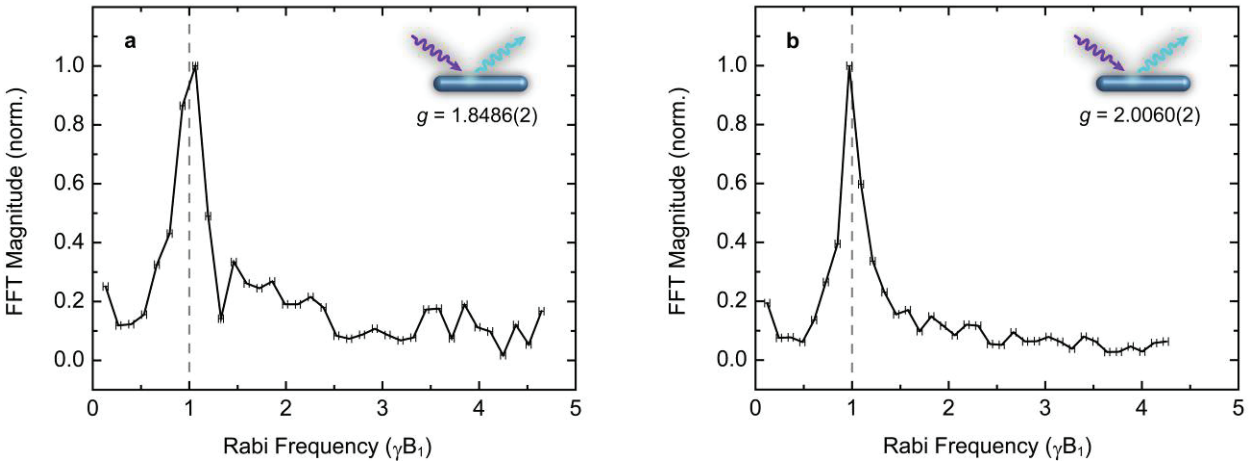

Figure S3: Frequency components of Rabi oscillations for both the $g \sim 1.84$ (a) and $g \sim 2.00$ (b) resonances of CdS nanorods. The frequency axis is scaled to γB_1, the Rabi frequency of a spin-½ paramagnetic center (marked by the vertical dashed line). There are no additional frequency components, demonstrating that each of these carriers is a spin-½ species and that the coupled pair of carriers experiences negligible exchange or dipolar coupling.

Measuring spin coherence with Hahn echoes

A lower limit on the spin dephasing time, T_2^*, of a paramagnetic center can be obtained by considering the amplitude decay of the Rabi oscillations. There are two primary mechanisms which artificially shorten coherence time in our system. One is due to the slight inhomogeneities in the oscillating magnetic field of the microwave radiation across the sample, B_1, which leads to a distribution of Rabi frequencies, $\Delta\Omega_R$. Another is due to the distribution of local nuclear magnetic moments perturbing the static magnetic field, B_0, experienced by the trapped carriers. This distribution leads to an additional detuning term in the Rabi

frequency, further increasing $\Delta\Omega_R$. This spread in frequencies evolves the system towards incoherent transitions between the two spin configurations more quickly, but can be overcome by taking advantage of microwave pulse techniques to reveal the true dephasing time of the system, T_2. The Hahn echo pulse sequence is particularly appropriate[9]. Since the observable in ODMR is permutation symmetry (i.e. bright or dark mutual spin configuration) and not polarization as in traditional magnetic resonance, we use a slightly modified version of this classic technique. A simple $\frac{\pi}{2}-\tau-\pi-\tau-\frac{\pi}{2}$ pulse sequence is illustrated schematically in Fig. S4a), where a π-rotation denotes a complete reflection in permutation symmetry for the system and is determined by the precession time measured in a Rabi oscillation. The dynamics involved are straightforward. The first $\frac{\pi}{2}$-pulse places the initially bright spin population into a superposition of bright and dark states. After a delay time, τ, in which the system dephases according to the distribution in Larmor frequencies arising from field inhomogeneities, a π-pulse is applied in order to reverse the Larmor precession of the system. This reversal effectively takes advantage of the time-reversal symmetry enforced by the long-time stability of the perturbing fields. The subsequent rephasing, or reversal in dephasing, takes place on a timescale equal to that of the initial delay, making the total dephasing time the system is subjected to 2τ. The second $\frac{\pi}{2}$-pulse is then applied in order to bring the remaining spin ensemble back to an observable state. By sweeping the $\frac{\pi}{2}$-pulse following the pulse sequence, a small change in the amplitude of transient response (i.e. the differential PL) is measured. This change is referred to as an echo, whose amplitude directly corresponds to the remainder of the initial population. By repeating this sequence and recording the echo as a function of 2τ, the loss of spin coherence is observed in the exponential decay of amplitude. Fig. S4b) illustrates this process by displaying some representative echoes using data for the CdS nanorod $g \sim 2.00$ center reproduced from the inset of Fig. 4b) in the main text.

We note that the uncertainty of the quoted spin coherence time of the $g \sim 2.00$ resonance is higher than that of the $g \sim 1.84$ resonance, not due to improved signal-to-noise in the latter, but because of a

complicated interference of the electron spin with nuclear magnetic moments. This substructure to the decay amplitude is apparent in Fig. S4b). It arises due to a phenomenon known as electron spin echo envelope modulation (ESEEM). Amplitude modulations of exponential decay of spin phase coherence would be expected to be present in the case of a finer structure splitting of the already Zeeman-split energy levels. These modulations do not prevent extraction of the decoherence time. With higher sensitivity, ESEEM should allow a precise chemical fingerprinting of the trap site in the future by providing information on local nuclear magnetic moments.

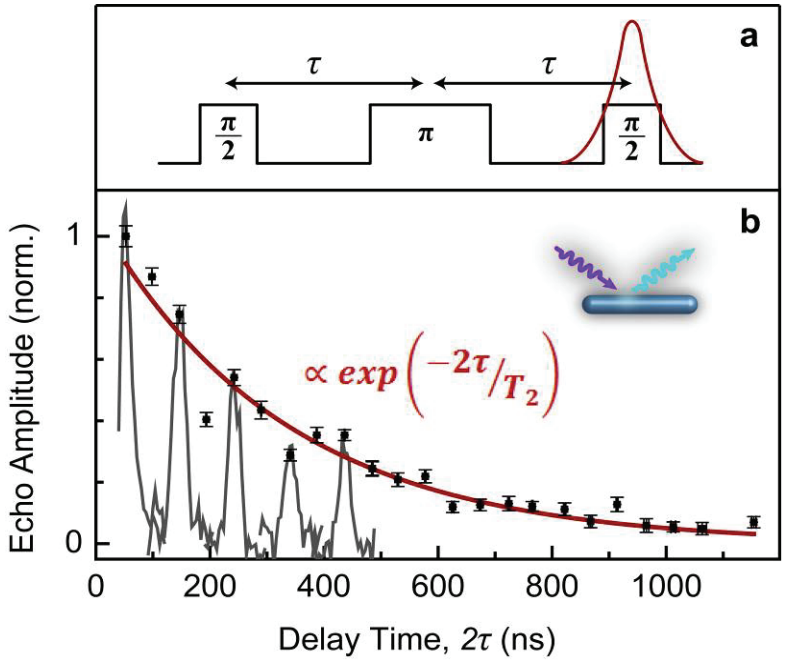

Figure S4: Hahn echo pulse sequence to extract the spin dephasing time. A $\frac{\pi}{2}$-pulse projects the dominant initial population into a superposition of bright and dark states. Decoherence due to a distribution in local Larmor precession frequencies is reversed by application of a π-pulse after a delay time τ. A second $\frac{\pi}{2}$-pulse projects the remaining superposition states (i.e. those which have not lost their spin phase information) back into a bright configuration.

Dependence of the resonance centers on excitation energy

In order to probe the energetic distribution of the trap centers, we studied the dependence of the CdSe/CdS tetrapod ODMR spectrum on excitation photon energy. This material system was chosen since excitation could be tuned from above the CdS arm band gap down to the absorption of the CdSe core while monitoring the resonance through the red-shifted PL of the CdSe core. Fig. S5 shows the results of this excitation sequence. The broad, central resonance significantly decreases in amplitude at 488 nm (2.541 eV) excitation compared to 458 nm (2.708 eV) excitation, and disappears completely at 514 nm (2.412 eV). The coupled-pair resonances ($g \sim 2.00$ and $g \sim 1.84$) remain intact, although some broadening is observed with decreasing excitation energy. This observation implies that the species represented by the central resonance has a unique relationship to the delocalized band-edge states of CdS, as compared to the $g \sim 2.00$ and $g \sim 1.84$ coupled-pair species, which exist over a much broader distribution of excitation energies. As commented on in the main text, this observation suggests that the narrow pair species both correspond to CdS surface states which can be populated even by direct excitation of the CdSe core slightly below the CdS band edge. Due to the presence of lattice strain at the heterojunction interface[10], carriers can still become trapped in the CdS even if the excitation energy lies below the band gap of the CdS nanorod. The involvement of lattice strain may explain the slight broadening of the $g \sim 2.00$ and $g \sim 1.84$ coupled-pair resonances with decreasing excitation energy. These resonances are comparatively narrow suggesting that they correspond to discrete atomic sites such as surface defects, organic ligands or the surrounding organic matrix. In contrast, the broad resonance can only be excited when the CdS is pumped above the band edge, suggesting that this species originates from bulk delocalized states in the CdS with substantial disorder broadening due to a wide range of chemical environments probed.

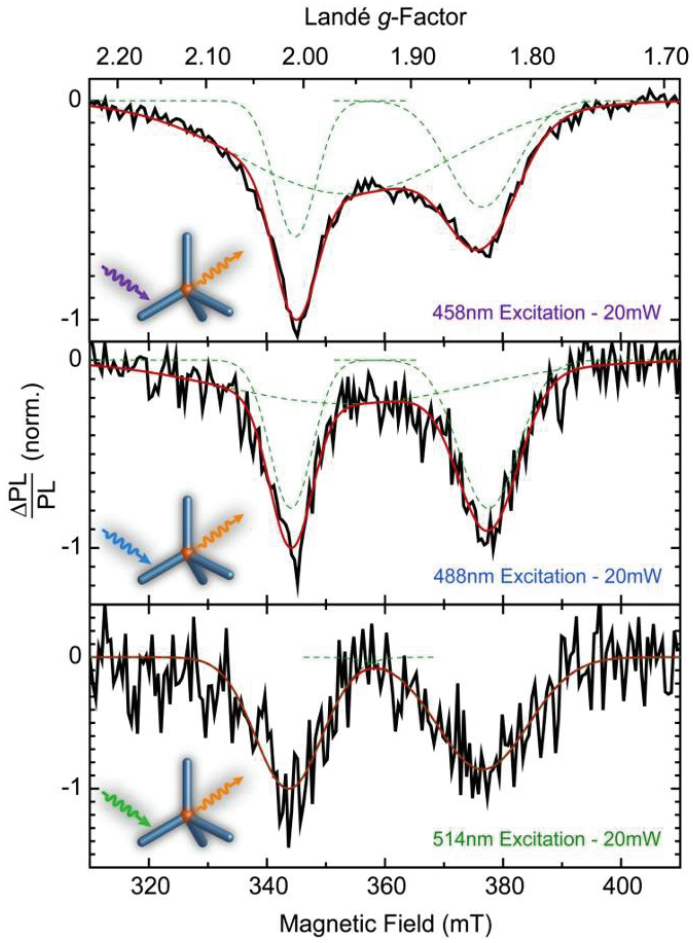

Figure S5: Dependence of tetrapod ODMR spectra on excitation energy. As excitation energy is decreased, the central resonance disappears, suggesting a close relationship to band-edge states. The coupled-pair resonances remain, shifting slightly in center position and broadening.

Discussion on the possible origin of the observed *g*=2 resonance

The resonance present in the CdS nanorods which is most closely aligned with the free-electron *g*-value is that at $g = 2.0060(2)$. Although the same center is observed through the CdSe core emission of the tetrapod structure, since the deep-level chemical defect of the CdS arm also emits at this energy (Fig. 2c), the exact resonance position is likely perturbed due to convolution with the resonance structure of the defect (Fig. 2d). To avoid this convolution we rely on the CdS nanorod data to most accurately assess the

features of the $g = 2.0060(2)$ resonance, since in this case the excitonic and defect states are spectrally well separated. In describing the nature of the $g \sim 2.00$ resonance, there are two possible models which are supported in the literature. One involves a photogenerated hole becoming trapped at the CdS surface in an undetermined chemical position[11]. Another possibility is that a charge becomes localized to an incorrectly-bonded surface-ligand site[12], or ejected from the nanoparticle into the surrounding organic matrix[13]. Both situations are suspected to constitute a type of charge trap[12]. Each of these situations is expected to result in a resonance position very close to that of the free-electron *g*-factor ($g \sim 2.0023$).

In the case of the photogenerated hole in CdS, Ref. 10 reported such a site which displayed an axial *g*-factor asymmetry with $g_{//} = 2.035$ and $g_{\perp} = 2.005$, where parallel and perpendicular refer to the alignment of principal *g*-factor axes with respect to the external magnetic field, $\vec{B}_0$. For a disordered ensemble of nanocrystals, each of these *g*-factor axes is randomly oriented with respect to $\vec{B}_0$ and so the spin resonance spectrum will display distinct peaks for each principal *g*-value, as well as a continuum of peaks between these values representing the linear combination of projections. Such a lineshape is referred to as an anisotropic powder pattern. In general, $g_{\perp}$ results in a higher degree of spin-polarization due to the larger number of axis-normal orientations expressed in the random distribution. This effect would give maximal resonant change in photoluminescence at $g_{\perp}$, as compared to $g_{//}$, which is very near to the situation we observe here.

In considering the second case, that of the charge localized to some organic material (either ligands or matrix), we also find good agreement between our measurements and the expected characteristics for such a material. Due to the extremely low levels of spin-orbit coupling, the *g*-factor of organic materials is found to be quite close to the free-electron value. Consequently, for a charge which is localized to a surface passivating organic ligand, a resonance very close to $g \sim 2.0023$ would be expected. In addition to the resonance position, the value for the T_2 coherence time determined is much longer than those

reported for similar inorganic quantum dots[14], yet is of the order of that measured in organic semiconductor systems[14]. Since neither the organic ligands nor the matrix are π-conjugated, it is not presently clear how their chemical structures would support charging, although defect centers respective to these materials are conceivable.

Discrimination between these two models remains difficult at this time without additional information. The level of inhomogeneous broadening and the overlap of the $g \sim 1.95$ resonance presently prevent us from resolving in detail any possible anisotropic features of this resonance. In the previous report of photogenerated holes in CdS[11], detailed information regarding the relative amplitude difference and line width difference between the $g_{\perp}$ and $g_{//}$ spectral positions is lacking. We therefore resort to using a single Gaussian line profile in order to represent this resonance as a type of first-order approximation. More parameter information is necessary (line widths and peak intensity ratios) to faithfully make use of a powder pattern fitting function in comparing these two models.

Resolving the ambiguity of chemical assignment for this resonance site could be carried out in at least two ways. One is in using an electron-spin-echo (ESE) detection scheme in order to map out the resonance structure. This technique allows one to independently measure the resonance structure of two overlapping species which have differing coherence times. The ability to separate out the overlapping $g \sim 1.95$ resonance may result in finer resolution of the $g \sim 2.00$ feature details and therefore resolve the issue of line shape anisotropy. A second method of resolving this issue is through taking advantage of the slight amplitude modulation which is likely to be present in the Hahn echo decay of this center, known as ESEEM (described above). By measuring this modulation with higher resolution, both in amplitude and echo delay spacing, the frequency components involved should allow discrimination between the trapped spin interacting with either a local H or Cd nuclear magnetic moment. Such a measurement would give a direct chemical fingerprint of the trap site position.

Supporting References

(1) Jones, M.; Lo, S. S.; Scholes, G. D. *Proc. Natl. Acad. Sci.* **2009**, *106* (9), 3011-3016.

(2) van Driel, A. F.; Nikolaev, I. S.; Vergeer, P.; Lodahl, P.; Vanmaekelbergh, D.; Vos, W. L. *Phys. Rev. B* **2007**, *75*, 035329.

(3) McCamey, D. R.; Lee, S.-Y.; Paik, S.-Y.; Lupton, J. M.; Boehme, C. *Phys. Rev. B* **2010**, *82*, 125206.

(4) Astashkin, A. V.; Schweiger, A. *Chem. Phys. Lett.* **1990**, *174*, 595–602.).

(5) Gliesche, A.; Michel, C.; Rajevac, V.; Lips, K.; Baranovskii, S. D.; Gebhard, F.; Boehme, C. *Phys. Rev. B* **2008**, *77*, 245206.

(6) Herring, T. W.; Lee, S.-Y.; McCamey, D. R.; Taylor, P. C.; Lips, K.; Hu, J.; Zhu, F.; Madan, A.; Boehme, C. *Phys. Rev. B* **2009**, *79*, 195205.

(7) Lee, S.-Y.; Paik, S.-Y.; McCamey, D. R.; Yu, J.; Burn, P. L.; Lupton, J. M.; Boehme, C. *Journal of the American Chemical Society* **2011**, *133*, 2019–2021.

(8) Efros, A.; Rosen, M.; Kuno, M.; Nirmal, M.; Norris, D.; Bawendi, M. *Phys. Rev. B* **1996**, *54*, 4843–4856.

(9) Hahn, E. L. *Phys. Rev.* **1950**, *297*, 580–594.

(10) Smith, A. M.; Nie, S. *Acc. Chem. Res.* **2010**, *43*, 190–200.

(11) Nakaoka, Y.; Nosaka, Y. *J. Phys. Chem.* **1995**, *99*, 9893–9897.

(12) Voznyy, O. *J. Phys. Chem. C* **2011**, *115*, 15927–15932.

(13) Efros, A. L.; Rosen, M. *Phys. Rev. Lett.* **1997**, *78* (6), 1110-1113.

(14) Whitaker, K. M.; Ochsenbein, S. T.; Smith, A. L.; Echodu, D. C.; Robinson, B. H.; Gamelin, D. R. *J. Phys. Chem. C* **2010**, *114* (34), 14467-14472.

(15) Baker, W. J.; Keevers, T. L.; Lupton, J. M.; McCamey, D. R.; Boehme, C. *Phys. Rev. Lett.* **2012**, *108*, 267601.